

## The Use of Grand Canonical Density Functional Theory Global and Local Reactivity Parameters to Study Electrochemical Processes in Energy Storage Materials

---

Claudia Islas-Vargas<sup>1,3</sup>, Alfredo Guevara-García<sup>2</sup>, Marcelo Galván<sup>1\*</sup>

<sup>1</sup>Departamento de Química, Universidad Autónoma Metropolitana Iztapalapa, Av. San Rafael Atlixco 186, Leyes de Reforma 1ra Secc, Iztapalapa, 09340, Ciudad de México, México.

<sup>2</sup>Departamento de Química, CONAHCYT-Universidad Autónoma Metropolitana Iztapalapa, Av. San Rafael Atlixco 186, Leyes de Reforma 1ra Secc, Iztapalapa, 09340, Ciudad de México, México.

<sup>3</sup>Sección de Química Analítica, Facultad de Estudios Superiores Cuautitlán, Universidad Nacional Autónoma de México, Cuautitlán Izcalli, México.

\*Corresponding author: Marcelo Galván, email: mgalvan@xanum.uam.mx

Received May 22<sup>nd</sup>, 2024; Accepted September 23<sup>rd</sup>, 2024.

DOI: <http://dx.doi.org/10.29356/jmcs.v69i1.2289>

**Abstract.** In this review a summary of the results obtained in a collaboration between electrochemists and theoretical physical chemists in the chemistry department of the Metropolitan Autonomous University Campus Iztapalapa in recent years is presented. The focus is on the study of materials involved in electrochemical storage devices such as batteries and capacitors, and in advance electrochemical oxidation reactions. Along this collaboration, the combination of density functional theory reactivity parameters within the Grand Canonical Density Functional Theory give rise to an alternative approach to follow redox processes in bulk materials and in solid-liquid interfaces. Along the review, we show how global and local softness emerge as suitable and ad hoc quantities to analyze electrochemical experiments. The use of local softness to distinguish “innocent” coordination environments from the active ones is exemplified with representative systems. A robust method to estimate quantum and total capacitances is described in the case of substituted graphene and is also applicable to other systems. Also, the introduction of an absolute approximate scale to characterize the redox properties of electrode-solvent systems is illustrated for a set of well-known surfaces of transition metal oxides.

**Keywords:** Grand canonical density functional theory; local and global softness; quantum capacitance; oxygen evolution.

**Resumen.** En esta revisión se presenta un resumen de los resultados obtenidos de una colaboración entre electroquímicos y fisicoquímicos teóricos del departamento de química de la Universidad Autónoma Metropolitana Unidad Iztapalapa en los últimos años. Se hace énfasis en el estudio de los materiales implicados en los dispositivos de almacenamiento electroquímico de energía, como baterías y capacitores, y en las reacciones de oxidación electroquímica avanzada. Se analiza el uso de los parámetros de reactividad definidos en la Teoría de Funcionales de la Densidad en su formulación Gran Canónica para estudiar procesos redox en el bulto de los materiales y en intercaras sólido-líquido. Se muestran ejemplos de cómo la blandura química global y local emergen como cantidades *ad hoc* para analizar el comportamiento de los materiales que participan en procesos electroquímicos. En particular, se muestra un ejemplo del uso de la blandura química local para distinguir, en procesos redox, los entornos de coordinación “inocentes” de los activos. Se describe también un método para estimar las capacitancias cuánticas y totales en el caso del grafeno sustituido y que es aplicable a intercaras sólido-líquido en general. Por otra parte, se ilustra, para un conjunto de superficies bien conocidas de óxidos de metales de transición, el uso de una escala absoluta aproximada para caracterizar en forma relativa las propiedades redox de los sistemas electrodo-disolvente.

**Palabras clave:** Teoría de Funcionales de la Densidad Gran Canónica; blanduras químicas global y local; capacitancia cuántica; evolución de oxígeno.

---

## Introduction

The application of electronic structure calculations for describing electrochemical processes has a long history and there are many theoretical efforts to obtain data and develop concepts to understand electrochemical phenomena.[1-24] In this context, efficient and precise prediction of redox potentials (RP) for extensive and varied sets of molecules and materials is crucial for the advancement of energy storage, wastewater treatment, conversion devices, catalysis, corrosion inhibition, amongst other applications. Efforts have been made to overcome these challenges by employing a range of computational approaches which aim to balance accuracy and computational efficiency such as density functional theory (DFT), semiempirical methods, wave function-based methods like Møller-Plesset perturbation theory (MP2) and coupled-cluster (CC), and machine learning approaches. Several publications are dedicated to this topic and readers are encouraged to consult the works made by Cramer and Truhlar [8,11], Arumugam and Becker [13], Pantazis et al. [12], Fornari and de Silva [9], Xue et al. [7], Neugebauer et al. [5] and Fedorov and Gryn'ova [10] for further insights.

Due to the complexity and size of the models needed to make an appropriate description of electrochemical systems, the most widely used methods in these applications are those based on DFT;[25] and ab-initio molecular dynamics based on DFT has been particularly useful to obtain RP. [1,2,14,15] Also, the simulation of electrochemical interfaces,[3] the evaluation of bulk properties of materials for energy storage,[6] and the study of electrocatalytic reactions [24] have reached remarkable standards.

DFT is not only a good calculational tool, alternative to the wave function approaches, but also, it is a powerful framework to connect chemical concepts with response properties defined within its mathematical structure;[26] along this research line there are successful developments to apply conceptual DFT (CDFT) defined quantities for studying electrochemistry. [4,16-23] The estimation of redox potentials using CDFT response function has been linked to Grand Canonical DFT (GCDFT) formalism since the pioneer works of Moens et al, [16,17] but there are approaches using the Canonical formulation of DFT too [18]. Direct applications of CDFT to electrochemical process have been done using the GCDFT [4,20] and the Canonical version of the theory. [19,21-23] As has been pointed out, the applications of GCDFT in the context of CDFT is an emerging research topic,[27] based on the recently developed mathematical framework;[28] and electrochemistry is in the front row of these kind of applications.

In recent years, there has been an effort between colleagues of the theoretical chemistry and electrochemistry groups in the Chemistry Department at the Universidad Autónoma Metropolitana, Unidad Iztapalapa (UAM-I) to collaborate for studying some aspects of electrochemistry processes. In this context, the scope of this review deals with the application of reactivity concepts defined in DFT to the analysis of electrochemical processes. It is pertinent to note that the objective of this work is to provide an overview of the advancements achieved within our research group, and it does not aim to offer a compilation of all the theories and concepts developed within this field throughout the years for the scientific community in general. Our aim is to analyze and assess the methods used, and the insights and progress generated by our group's research efforts in understanding how electronic structure calculations intersect with electrochemistry.

In general, an electrochemical process involves a charge transfer; and this transfer can involve two different kinds of charged particles, electrons and/or ions. For this reason, in the simulation of such chemical events, it is necessary to treat the systems involved as open systems from the point of view of ions and electrons. So, in principle one must use a Grand Canonical formalism to treat ions and electrons. In batteries, a key process to analyze in electrode materials is the redox changes induced during the intercalation or deintercalation of ions in the crystal framework; fortunately, this process can be studied with periodic conditions methods under electroneutral conditions using a model of the bulk material which is feasible to treat with standard methods for the evaluation of the electronic structure of solids.[6] For the theoretical treatment of the solid-liquid interfaces, that are relevant systems in electrochemistry, what is needed is the study of a charged surface in contact with a solvent containing ions at a certain concentration. A reasonable representation of such a complex system needs

to have a suitable model of a surface in contact with the electrolyte and allow the solid surface to be charged as a response to an imposed potential. If one must use periodic conditions, the treatment of charged quantum systems requires, in addition to what was mentioned above, to generate neutral unit cells to avoid the long range inter cells coulombic contributions. There are two ways of generating electroneutral unit cells, on the one hand, it is possible to use a compensating jellium media with the same charge of the solid surface in calculations at a fixed number of electrons; on the other hand, one may include a solvent model with dipole and monopole responses that compensate the induced charge on the solid surface. This second approach is the one used in our group to describe solid-liquid interfaces. In addition, to reduce the size of the model, a half cell connected to an electrons bath at a certain chemical potential is used. This situation requires treating the quantum system as an open one with respect to the electrons and our approach avoids a treatment of an open system with respect to ions: in other words, the treatment of solid-liquid interfaces is restricted to be grand canonical for electrons but not for ions. Therefore, the use of the Grand Canonical Finite Temperature Density Functional Theory (GCDFT) [29,30] is mandatory. To our knowledge, the Joint Density Functional Theory (JDFT) [31-38] developed by the group of Professor Arias fulfills all the key physical aspects to take into account for studying the electronic structure of an electrode in a solid-liquid interface in the context of the GCDFT. In this review we will summarize the efforts of our research group to evaluate response quantities defined in the GCDFT chemical reactivity formalism and the application of them to study electron transfer processes in solids, especially in active materials for batteries, and in solid-liquid interfaces to describe electrochemical capacitors and advanced electrochemical oxidation reactions. Accordingly, the review is organized as follows. Then the use of local softness to predict oxygen evolution reactions in alkali-ion batteries is explained. As the use of a robust solvent model in the study of solid-liquid electrochemical systems is required, we describe JDFT formalism with emphasis in the solvent model in "Joint Density Functional Theory" section; after that the results obtained using this solvent model to calculate the quantum capacitances of graphene are displayed, followed by a comparison of redox properties of several solid-liquid interfaces of metal oxides. Finally, the conclusions are depicted.

## Grand Canonical DFT Formalism

In the Grand Canonical Finite Temperature Density Functional Theory (GCDFT) [29,30] the Grand Potential,  $\Omega[\mu, V(\mathbf{r}), T]$ , has the central role instead of the Total Energy,  $E[N, V(\mathbf{r})]$ . The Grand Potential has the external potential,  $V(\mathbf{r})$ , the chemical potential of the electron reservoir,  $\mu$ , and the temperature,  $T$ , as natural variables. To emphasize the density dependence and the fact that in the GCDFT this property is an ensemble average, one may define the grand potential as:[39]

$$\Omega[\langle\rho(\mathbf{r})\rangle] = E[\langle\rho(\mathbf{r})\rangle] - TS[\langle\rho(\mathbf{r})\rangle] - \mu\langle N \rangle \quad (1)$$

In this notation  $\mu$  and  $\langle\rho(\mathbf{r})\rangle$  are the chemical potential of the electrons reservoir (bath) and the ensemble average electron density respectively; and  $\langle N \rangle$  is the ensemble average of the number of electrons,  $\langle N \rangle = \int \langle\rho(\mathbf{r})\rangle d\mathbf{r}$ . By identifying the Helmholtz free energy,  $A$ , as the two first terms of the right side of Eq. 1, one may rewrite this equation as

$$\Omega[\mu, V(\mathbf{r}), T] = A - \mu\langle N \rangle \quad (2)$$

That is the Legendre transformation of  $A$  with respect to  $\langle N \rangle$ . By this transformation there is an implicit formal change from the dependence of  $A$  on  $\langle N \rangle$  to a dependence on  $\mu$ . Eq. 2 is a formal definition of the Grand Potential in the context of the GCDFT formalism. In a section below a detailed description of the Helmholtz free energy is developed within the Joint Density Functional Theory.

According to Eq. 2, in the GCDFT any change in the grand potential in terms of its natural variables at constant temperature is given by

$$\delta\Omega = -\langle N \rangle d\mu + \int \langle \rho(\mathbf{r}) \rangle \delta V(\mathbf{r}) d\mathbf{r} \quad (3)$$

Within the formalism outlined above the concept of chemical softness was developed as global, local and non-local quantities:[28,40]

$$S \equiv \left( \frac{\partial \langle N \rangle}{\partial \mu} \right)_{T, V(\mathbf{r})} \quad (4)$$

$$S(\mathbf{r}) \equiv \left( \frac{\partial \langle \rho(\mathbf{r}) \rangle}{\partial \mu} \right)_{T, V(\mathbf{r})} = - \left( \frac{\partial \langle N \rangle}{\partial V(\mathbf{r})} \right)_{T, \mu} \quad (5)$$

$$S(\mathbf{r}, \mathbf{r}') \equiv - \left( \frac{\delta \langle \rho(\mathbf{r}') \rangle}{\delta V(\mathbf{r})} \right)_{T, \mu} \quad (6)$$

The equality in Eq. 5 is a Maxwell relation obtained from Eq. 3. By using Eqs. 3-5, a change in the average number of electrons is written as

$$d\langle N \rangle = S d\mu - \int S(\mathbf{r}) \delta V(\mathbf{r}) d\mathbf{r} \quad (7)$$

As one may conclude by analyzing Eq. 7, global,  $S$ , and local  $S(\mathbf{r})$  softness are reactivity parameters related to the capability of the system to perform electron transfer. They can be related to fluctuations in the number of electrons and the electron density. Also, softness is a concept related to polarizability.[41] In addition, the softness kernel,  $S(\mathbf{r}, \mathbf{r}')$ , is connected to the linear response function. The usefulness of softness in the interpretation of reactive trends in molecules and solids is well documented.[26] One interesting property of the hierarchy of softness quantities is that they are related by simple integration: local softness is the integral of the softness kernel with respect to one of the two position variables; and global softness is equal to the space integral of local softness. As the Fukui function,[42] local softness is an extensive property in the sense that any spatial partition of the density gives rise to an equivalent partition of the property; thus, one can define regional softnesses within a chemical system. For the purposes of this review, we will develop applications of softness in electron transfer processes in solids, especially in active materials for batteries, and in solid-liquid interfaces to describe electrochemical capacitors and advanced electrochemical oxidation reactions.

## Local softness to predict oxygen evolution reactions in alkali-ion batteries

Redox properties of active materials are fundamental to understanding the performance of alkali-ion batteries. Electrons flow between the positive and the negative electrodes during the charge and discharge processes while the alkali ions are intercalated in the active materials to compensate for the generated charge, [43,44] see Fig. 1. Commonly used active materials, for the cathodes, usually contain metal ions bound to ligands.[45] These ligands can be classified as actor or spectator ligands according to their participation in the localization or delocalization of the added electrons in the host material,[4] in other words, according to their contribution to the bands involved in the redox process. These two cases are schematically represented in Fig. 1. For spectator ligands, the acquired electrons are mainly located over the reduced metal centers. In these cases, it seems that electrostatic interactions are all you need to explain or predict the experimental intercalation voltages,[4] but in some cases we have found that dispersion interactions may be needed to reproduce the

observed values.[46] When actor ligands appear the electrons are distributed in bands with metal and ligand character. One way to evaluate this contribution is to analyze the partial density of states (PDOS) near de Fermi level. As shown by Johannes et al.,[47] this can also be used to evaluate the stability of Li-ion active cathode materials related to oxygen gas evolution. The main idea is to compute the PDOS and analyze their contribution to the total density of states near the Fermi level. If the DOS has a higher contribution of states from oxygen atoms i.e. a higher oxygen character, the cathode material is prone to suffer oxygen evolution reactions and if the DOS has a higher metal character, oxygen evolution reactions may not occur. Because their analysis depends on the quality of the description of the states near the Fermi level, they pointed out the need to use a range separated hybrid functional for this goal.[48] With this in mind, two of the authors[49] proposed the use of local softness[40, 50] as an alternative way to obtain information on how redox processes happen in this kind of materials. In the context of solids and using a Taylor expansion up to first order to evaluate the difference in electron density between a system where its electron density is modified as a result of a change in the chemical potential from a reference one and a system at that reference chemical potential, one can derive a finite difference approximation for the local softness as:[49]

$$S(\mathbf{r}) \approx \frac{1}{\Delta\mu} \int_{\mu_0}^{\mu_0+\Delta\mu} g(\mathbf{r}, \varepsilon, \mu_0) d\varepsilon + \int_{V(\mathbf{r}), \mu=\mu_0}^{\mu_0+\Delta\mu} \left( \frac{\partial g(\mathbf{r}, \varepsilon, \mu)}{\partial \mu} \right) d\varepsilon \quad (8)$$

where  $S(\mathbf{r})$  is the local softness,  $\mu$  is the chemical potential, and  $g(\mathbf{r}, \varepsilon, \mu)$  is the local density of states. It should be remembered that the change in the electron density  $\rho(\mathbf{r})$ , while changing  $\mu$ , is evaluated at constant external potential  $V(\mathbf{r})$ . If the second term of the above equation, that accounts for the relaxation of the local density of states when the chemical potential is changed, is ignored, an expression for the local softness within the rigid band approximation can be obtained:

$$S(\mathbf{r}) \approx \frac{1}{\Delta\mu} \int_{\mu_0}^{\mu_0+\Delta\mu} g(\mathbf{r}, \varepsilon, \mu_0) d\varepsilon \quad (9)$$

The sign of the change in the chemical potential  $\Delta\mu$  determines if the system is gaining or losing electrons.  $\Delta\mu$  is selected to account for the loss or gain of one electron, according to the next equation:

$$\int_{\Omega} \int_{\varepsilon_f}^{\varepsilon_f+\Delta\mu} g(\mathbf{r}, \varepsilon, \mu_0) d\varepsilon d\mathbf{r} = 1.0 \quad (10)$$

where the integral over  $\mathbf{r}$  is done in the unit cell volume,  $\Omega$ . As in this case the processes to analyze are in bulk, the influence of the solvent is not included.

The local softness computed for  $\text{LiFePO}_4$  under the conditions described above is shown in Fig. 2. As can be seen from that figure, the yellow surfaces that represent the local softness lie over the iron atoms indicating that if one tries to remove an electron from  $\text{LiFePO}_4$ , that electron might come from those regions.  $\text{LiFePO}_4$  is a material with spectator ligands. One of the advantages of using the local softness to analyze the oxygen character of the states around the Fermi level of different compounds is that a semiquantitative comparison can be made between different systems. For example, Fig. 3 shows the local softness for  $\text{Li}_2\text{CuO}_2$  and  $\text{LiCuO}_2$ . These two materials have actor ligands as can be appreciated in the last figure, where it is clear that electrons can be removed not only from the metal center but also from the oxygen atoms coordinated to them. As shown by the size of the local softness plots, it can be inferred that it is easier to remove electrons from the oxygen atoms in  $\text{LiCuO}_2$  compared to  $\text{Li}_2\text{CuO}_2$ . In summary, computing the local softness in cathode materials to understand the electronic states near the Fermi level is an alternative way that gives a direct insight of the nature of the states involved in redox processes.

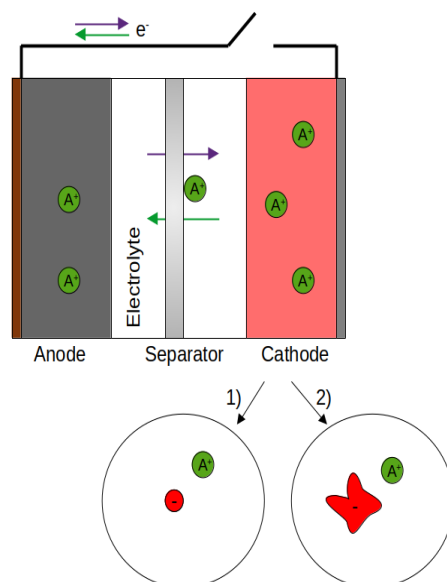


**Fig. 1.** Schematic representation of the components of an alkali ion battery, the intercalation and deintercalation processes that occur during the charge and discharge of the battery and the two possible scenarios where the ligands are involved in the localization or delocalization of the electrons of the reduced state of the metal centers.

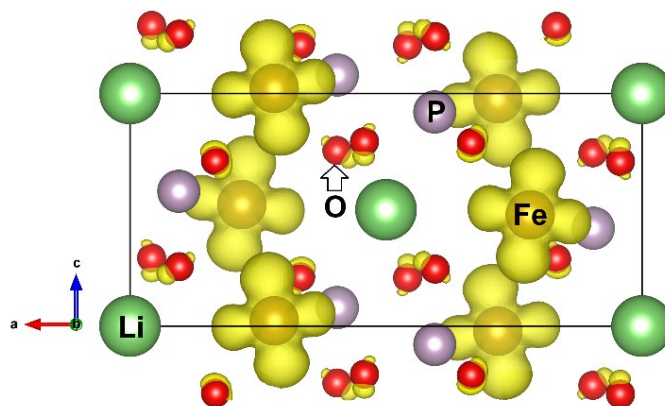


**Fig. 2.** Local softness 0.354 a.u. isosurface plot for LiFePO<sub>4</sub>. The  $S(r)$  isosurface is shown in yellow. This figure is not part of the governing open access license but has been reproduced with permission from Springer Nature Customer Service Centre GmbH, from Perea-Ramírez, L. I.; Guevara-García, A.; Galván, M. *Journal of Molecular Modeling* **2018**, 24, 227, Springer Nature. The rights of this figure are owned by a third party.

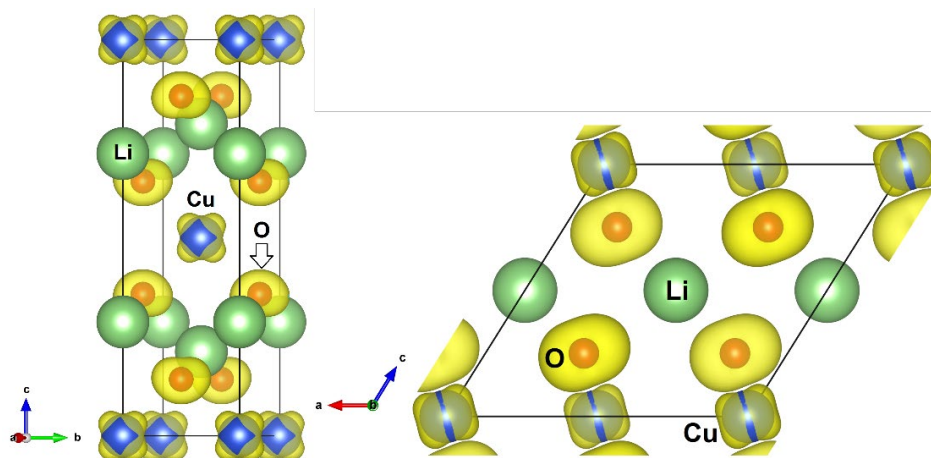


**Fig. 3.** Local softness 0.354 a.u. isosurface plots for  $\text{Li}_2\text{CuO}_2$  (left) and  $\text{LiCuO}_2$  (right). The  $S(\mathbf{r})$  isosurfaces are shown in yellow. This figure is not part of the governing open access license but has been reproduced with permission from Springer Nature Customer Service Centre GmbH, from Perea-Ramírez, L. I.; Guevara-García, A.; Galván, M. *Journal of Molecular Modeling* **2018**, 24, 227, Springer Nature. The rights of this figure are owned by a third party.

## Joint Density Functional Theory

In electrochemical experiments, solvents are involved in stabilizing and allowing the movement of the ions between electrodes, modifying the thermodynamics and kinetics of the reactions taking place on the electrodes [51] or affecting properties like capacitance in supercapacitors [52], so, in some cases is unavoidable to include their effects to correctly explain or describe them.

The Joint Density Functional Theory (JDFT) [53] formalism is designed to treat electrochemical systems from the perspective of solid-state methods that use periodic conditions. It provides a framework where the system is separated into a solute, this can be a surface or a molecule, and the solvent which can be an electrolyte solution.

The variational principle associated to this theory, corresponds to the minimization of the Helmholtz free energy,  $A$ :

$$A = \min_{\{\rho(\mathbf{r}), \rho_\alpha(\mathbf{r})\}} \left( \tilde{A}_{JDFT}[\rho(\mathbf{r}), \{\rho_\alpha(\mathbf{r})\}] + \int d\mathbf{r} V(\mathbf{r})\rho(\mathbf{r}) + \sum_\alpha \int d\mathbf{r} V_\alpha(\mathbf{r})\rho_\alpha(\mathbf{r}) \right) \quad (11)$$

where  $\rho(\mathbf{r})$  is the electronic density,  $\{\rho_\alpha(\mathbf{r})\}$  is the set of nuclear densities associated with the electrolyte solution,  $V(\mathbf{r})$  and  $V_\alpha(\mathbf{r})$  are the external potential due to the nuclei of the solute and the ones applied to the liquid components, respectively. The  $\tilde{A}_{JDFT}[\rho(\mathbf{r}), \{\rho_\alpha(\mathbf{r})\}]$  is a universal functional independent of  $V(\mathbf{r})$  and  $V_\alpha(\mathbf{r})$ ; it includes the contributions of the interaction between solute and the electrolyte solution. As the solute is treated using the electronic DFT in the Kohn-Sham Mermin formalism, this last functional can be written as:

$$\begin{aligned} \tilde{A}_{JDFT}[\rho(\mathbf{r}), \{\rho_\alpha(\mathbf{r})\}] \\ = \sum_i \left( \frac{f_i}{2} \int d\mathbf{r} |\nabla\psi_i(\mathbf{r})|^2 - \text{TS}(f_i) \right) + E_H[\rho(\mathbf{r})] + E_{XC}[\rho(\mathbf{r})] \\ + \tilde{A}_{diel}^i[\rho(\mathbf{r}), \{\rho_\alpha(\mathbf{r})\}] \end{aligned} \quad (12)$$

where  $E_H$  and  $E_{XC}$  are the functionals containing the Coulombic interactions between electrons and nuclei and the exchange-correlation functional, respectively. Here the entropy  $S$ , has the independent particle form  $S(f) = -f \ln(f) - (1 - f) \ln(1 - f)$  and the occupations are given by the Fermi distribution:

$$f_i = \frac{1}{1 + \exp\left(\frac{\varepsilon_i - \mu}{T}\right)} \quad (13)$$

where  $\varepsilon_i$  are the eigenvalues of the Kohn-Sham equations. The  $\tilde{A}_{diel}[\rho(\mathbf{r}), \{\rho_\alpha(\mathbf{r})\}]$  functional depends on the average densities of the nuclei of the solvent and it also contains the solute-electrolyte interactions related to the average electron density and average solvent densities.

There are different approaches to treat the term  $\tilde{A}_{diel}$ . The first approximation consists of treating only the solute quantum mechanically; in this way, the average densities of the solvent nuclei are obtained from a formalism based on classical mechanics. There is a series of approximations involving various levels of treatment for the solvent ranging from density functional models for liquids to continuous solvent models. In this review only results obtained by continuous solvent models are considered.

**Continuous Solvent Model.** The effects of the solvent can be treated explicitly, implicitly or in a combination of both. In the case of treating them explicitly, a detailed description of the solvent needs the inclusion of several of its molecules in the calculation, however this procedure has its limitations since each explicit water molecule adds degrees of freedom making it more computationally demanding. With the purpose in mind of reducing the computational costs, several approaches have emerged to describe the solvent implicitly. To delve into the specifics of the methods and formulations, readers are encouraged to refer to the review articles covering this topic.[54-57]

**The Polarizable Continuum Model (PCM).** This model comprises simplified theories that consider the interactions between the solute and the liquid by placing the electronic system immersed in a continuous dielectric without structure, simulating solvation effects by generating a cavity whose shape and size can be described in various ways. Within the cavity, the solute's charge distribution polarizes the continuum, which in turn redistributes the solute's charge.[38,56]

In the context of the JDFT, the solvent model can be defined by approximating the free energy functional of the solvated electronic system as follows:

$$\tilde{A}_{JDFT}[\rho(\mathbf{r}), \{\rho_\alpha(\mathbf{r})\}] = \underbrace{A_{HKM}[\rho(\mathbf{r})]}_{\text{solute}} + \underbrace{\Phi_{liq}[\{\rho_\alpha(\mathbf{r})\}]}_{\text{liquid/electrolyte}} + \underbrace{\Delta A[\rho(\mathbf{r}), \{\rho_\alpha(\mathbf{r})\}]}_{\text{coupling}} \quad (14)$$

where  $A_{HKM}[\rho(\mathbf{r})]$  is the Hohenberg-Kohn-Mermin functional[29,30] of the solute depending on the electron density,  $\Phi_{liq}[\{\rho_\alpha(\mathbf{r})\}]$  is the exact free energy functional of the liquid that depends on the average densities of the solvent nuclei, and  $\Delta A[\rho(\mathbf{r}), \{\rho_\alpha(\mathbf{r})\}]$  is the free energy that captures the solute-solvent interactions. These can be approximated in different ways. Under the Kohn-Sham formulation,[58] the first term on the right-hand side can be approximated with different levels of theory for the exchange and correlation energy. For the second term, a classical density functional for liquids can be employed, and the last term can be separated by identifying contributions attributed to effects such as the mean-field electrostatic interaction and the ones dominated by electronic repulsion and dispersion. The  $A_{diel}$  functional can be defined as the sum of these last two terms:

$$A_{diel}[\rho(\mathbf{r})] \equiv \Phi_{liq}[\{\rho_\alpha(\mathbf{r})\}] + \Delta A[\rho(\mathbf{r}), \{\rho_\alpha(\mathbf{r})\}] \quad (15)$$

One can rewrite this functional to distinguish the different contributions:

$$\begin{aligned}
A_{diel}[\rho(\mathbf{r})] = & A_{\varepsilon}[s_{cav}(\mathbf{r}), \varepsilon(\mathbf{r})] + A_{\kappa}[s_{cav}(\mathbf{r}), \{\rho_{\alpha}(\mathbf{r})\}] \\
& + \int d\mathbf{r} \int d\mathbf{r}' \frac{\rho_{liq}(\mathbf{r}')}{|\mathbf{r} - \mathbf{r}'|} \left( \rho_{el}(\mathbf{r}) + \frac{\rho_{liq}(\mathbf{r})}{2} \right) + A_{cav}[s_{cav}(\mathbf{r})] \quad (16) \\
& + A_{disp}[s_{cav}(\mathbf{r})]
\end{aligned}$$

where  $A_{\varepsilon}[s_{cav}(\mathbf{r}), \varepsilon(\mathbf{r})]$  represents the free energy functional that captures the dielectric response corresponding to the electrostatic interaction of a fluid composed of neutral molecules, while  $A_{\kappa}[s_{cav}(\mathbf{r}), \{\rho_{\alpha}(\mathbf{r})\}]$  represents the contribution to the free energy from the electrolyte ions if they are present in the solution. The densities of the solvent molecules and ions are modulated by the function determining the cavity,  $s_{cav}(\mathbf{r})$ , which in turn is determined by the electronic density. The third term on the right-hand side of the equation is the mean-field electrostatic interaction of the liquid's bond charge,  $\rho_{liq}(\mathbf{r})$ , with itself and with the total charge density of the electronic system,  $\rho_{el}(\mathbf{r})$ , where  $\rho_{liq}(\mathbf{r}) = \rho_{\varepsilon}(\mathbf{r}) + \rho_{\kappa}(\mathbf{r})$  is the sum of the contribution from the charge associated with the dielectric response,  $\rho_{\varepsilon}(\mathbf{r})$ , and the ionic contribution,  $\rho_{\kappa}(\mathbf{r})$ , whereas  $\rho_{el}(\mathbf{r}) = \rho(\mathbf{r}) + \rho_{nuc}(\mathbf{r})$  is the sum of the electronic density and the density of the solute nuclei, respectively. The last two terms of the equation depend on the cavity function and capture the effects of cavitation,  $A_{cav}[s_{cav}(\mathbf{r})]$ , and dispersion,  $A_{disp}[s_{cav}(\mathbf{r})]$ , of the solute-solvent interaction.

The PCM model, in its linear response approximation, considers the effects of ionic and dielectric responses of the liquid to be linear and local, so that the dipole moment of the solvent molecule,  $\rho_{mol}$ , interacting with the total electrostatic potential  $\phi(\mathbf{r})$ , is much smaller than the temperature  $\rho_{mol}|\nabla\phi(\mathbf{r})| \ll k_B T$  and that the ionic response is approximately linear when  $Z|\nabla\phi(\mathbf{r})| \ll k_B T$ , where  $Z$  is the charge of the ion and  $k_B$  is the Boltzmann constant. Thus, we can write the following expression:

$$A_{\varepsilon} + A_{\kappa} \approx \frac{1}{4\pi} \int d\mathbf{r} s_{cav}(\mathbf{r}) \left[ (\varepsilon_b - 1) \frac{|\nabla\phi(\mathbf{r})|^2}{2} + \kappa^2 \frac{\phi^2(\mathbf{r})}{2} \right] \quad (17)$$

with the corresponding bound charge density,

$$\rho_{liq}(\mathbf{r}) = \frac{1}{4\pi} [(\varepsilon_b - 1)\nabla \cdot (s_{cav}(\mathbf{r})\nabla\phi(\mathbf{r})) - \kappa^2 s_{cav}(\mathbf{r})\phi(\mathbf{r})] \quad (18)$$

where  $\kappa = \sqrt{4\pi \sum N_i Z_i^2 / T}$  is the inverse of the Debye screening length in vacuum.

The Euler-Lagrange equation for this functional, when simplified under linear response conditions with respect to the independent variable  $\phi(\mathbf{r})$ , resembles the modified Poisson-Boltzmann equation, (or alternatively, the Helmholtz equation in scenarios involving electrolytes where  $\kappa$  does not equal zero)

$$\nabla^2 \phi(\mathbf{r}) + (\varepsilon_b - 1)\nabla \cdot (s_{cav}(\mathbf{r})\nabla\phi(\mathbf{r})) - \kappa^2 s_{cav}(\mathbf{r})\phi(\mathbf{r}) = -4\pi\rho_{el}(\mathbf{r}) \quad (19)$$

Finally, taking the solution to the electrostatic potential from this last equation and making substitutions, we get the equilibrium value of the  $A_{diel}$  functional in the linear response limit,

$$\begin{aligned}
A_{diel}[s_{cav}(\mathbf{r}), \phi(\mathbf{r})] \\
= & A_{cav}[s_{cav}(\mathbf{r})] + A_{disp}[s_{cav}(\mathbf{r})] \\
& + \frac{1}{2} \int d\mathbf{r} \rho_{el}(\mathbf{r}) \left( \phi(\mathbf{r}) - \int d\mathbf{r}' \frac{\rho_{el}(\mathbf{r}')}{|\mathbf{r} - \mathbf{r}'|} \right) \quad (20)
\end{aligned}$$

Therefore, under this approximation,  $A_{diel}$  is a functional of the total electrostatic potential and the cavity shape function. In general terms, the above description corresponds to a PCM that includes the effects

of an electrolyte. The inclusion of the ionic screening,  $\kappa \neq 0$ , define an unambiguous point of reference for the eigenvalues, consequently any solvent model with this characteristic defines a practical zero for all the systems treated. This opens the possibility of direct comparison of eigenvalues between different systems.

**CANDLE model.** One of the most successful PCM models used in the context of the GCDFT theory applied to electrochemistry problems is called CANDLE. This solvent model has the capability to describe the solvation energy for positive and negative charged systems, a characteristic quite appealing for treating electrochemical processes. Also, CANDLE describes appropriately cavitation free energies for solutes of positive, negative and zero curvature: invaginations, droplets, and planar interfaces. One key feature of this solvent model is the use of a finite thickness shell as the cavity border controlled by a form factor. Thus, the transition from the solute to the solvent is not sharp; in addition, the distance of the border crust with respect to the solute is adjusted according to the value of the electric field generated by the total density of the solute along the direction of the gradient of the electron density; as a consequence the shell position is different for anionic than for cationic regions. This extra adaptability of the solvent model is responsible for giving the same accuracy for solvation energies of cationic and anionic solutes, an important property to describe oxidation and reduction electrochemical processes with equal quality.

The CANDLE model builds upon the SALSALSA[31] solvation model (Spherically Averaged Liquid Susceptibility), with some modifications to the definition of the cavity shape function and the dispersion contribution. In the case of CANDLE the cavity shape function is

$$s_{\text{cav}}(\mathbf{r}) = \frac{1}{2} \operatorname{erfc} \ln \left\{ \frac{Z_{\text{val}} \bar{\rho}(\mathbf{r})}{\rho_c^{\text{eff}}} \right\} \quad (21)$$

where  $\bar{\rho}(\mathbf{r})$  is the convolution of the electron density of the solute,  $\rho(\mathbf{r})$ , and a spherical model of the molecular electron density of the solvent,

$$w_{\text{liq}}(\mathbf{r}) \equiv \frac{1}{(\sigma_{\text{liq}} \sqrt{2\pi})^3} \exp \frac{-r^2}{2\sigma_{\text{liq}}^2} \quad (22)$$

$Z_{\text{val}}$  is the number of electrons of the solvent molecule and  $\sigma_{\text{liq}}$  is adjusted so that the width of the gaussian function is related to the effective van der Waals radius of the solvent molecule. The quantity  $\rho_c^{\text{eff}}$  depends on the electric field associated to the total electron density,  $\rho_{\text{el}}(\mathbf{r}) = \rho(\mathbf{r}) + \rho_{\text{nuc}}(\mathbf{r})$ , and on an adjustable parameter,  $\rho_{\text{cav}}$ , that controls the differences between positive and negative regions of the solute. According to Eq. 21 the border between solute and solvent is not a surface but a crust where the width depends on the convolution density,  $\bar{\rho}(\mathbf{r})$ , and the distance to the solute is fixed by  $\rho_c^{\text{eff}}$ .

The cavity shape function described above is used directly to evaluate the dispersion contribution to solute-solvent interaction according to the equation:

$$A_{\text{disp}}[s_{\text{cav}}(\mathbf{r})] = -\sqrt{C_{\text{6eff}}} N_{\text{bulk}} \sum_i \int d\mathbf{r} (w_{\text{liq}} * s_{\text{cav}})(\mathbf{r}) \times \frac{\sqrt{C_{6i}}}{|\mathbf{R}_i - \mathbf{r}|^6} f_{\text{dmp}} \left( \frac{|\mathbf{R}_i - \mathbf{r}|}{R_{0i}} \right) \quad (23)$$

where  $C_{6i}$  and  $R_{0i}$  are the parameters of the DFT-D2 method of Grimme[59] for the  $i$ th atom of the solute at position  $\mathbf{R}_i$ , and  $f_{\text{dmp}}$  is the short-range damping function.  $N_{\text{bulk}}$  is the bulk number density of the solvent. To represent the solvent and generalize to non-spherical molecules, a distribution of polarizable oscillators given by  $w_{\text{liq}}(\mathbf{r})$  is employed, with  $\sqrt{C_{\text{6eff}}}$  an empirical parameter representing an effective dispersion coefficient, and  $s_{\text{cav}}(\mathbf{r})$  is the function that modulates this distribution. The notation  $(w_{\text{liq}} * s_{\text{cav}})(\mathbf{r})$  indicates the convolution of the functions.

For the evaluation of the dielectric and ions response, it is defined a dielectric shape function that is modulated by a sort of effective electrostatic radius,  $\eta$ , by using a convolution:

$$s'_\varepsilon(\mathbf{r}) \equiv (w_\eta * s_{\text{cav}})(\mathbf{r}) \quad (24)$$

$$w_\eta(\mathbf{r}) \equiv \frac{\delta(r - \eta)}{4\pi\eta^2} \quad (25)$$

The rationale of this change in the shape function is that the ions have a different average distance to the solute than the van der Waals interactions. Thus  $\eta$  becomes an adjustable parameter in CANDLE model. This imply that  $s'_\varepsilon(\mathbf{r})$  substitutes  $s_{\text{cav}}(\mathbf{r})$  in Eqs. 17-19.

In CANDLE, the contribution of cavitation is expressed by

$$\begin{aligned} A_{\text{cav}}[s_{\text{cav}}(\mathbf{r})] = & p \int d\mathbf{r} (1 - \bar{s}(\mathbf{r})) \\ & + N_{\text{bulk}} T \int d\mathbf{r} \bar{s}(\mathbf{r}) (1 - \bar{s}(\mathbf{r})) \left[ \bar{s}(\mathbf{r}) + (1 - \bar{s}(\mathbf{r})) \gamma \right. \\ & \left. + 15 \bar{s}(\mathbf{r}) (1 - \bar{s}(\mathbf{r})) \left( \frac{\sigma_{\text{bulk}}}{N_{\text{bulk}} T R_{\text{vdW}}} - \frac{1 + \gamma}{6} \right) \right] \end{aligned} \quad (26)$$

where  $p$  and  $T$  are the pressure and temperature of the fluid with  $\gamma \equiv \ln \frac{N_{\text{bulk}} T}{p_{\text{vap}}} - 1$ , and  $p_{\text{vap}}$  the vapor pressure of the solvent. In this model, the term  $\bar{s}(\mathbf{r}) = (w_{\text{vdW}} * s_{\text{cav}})(\mathbf{r})$  is a convolution of the cavity shape function with a spherical weighting function,  $w_{\text{vdW}}(\mathbf{r}) = \delta(r - \sigma_{\text{vdW}}) / 4\pi\sigma_{\text{vdW}}^2$ , which employs the solvent radius as  $\sigma_{\text{vdW}} = 2R_{\text{vdW}}$  where  $R_{\text{vdW}}$  is the van der Waals radius of the solvent molecule. This form of the cavitation free energy has no adjustable parameters and describes the energy associated to the formation of a cavity with an arbitrary shape; and it only depends on experimental data specific to the solvent. For this reason, CANDLE has three parameters that must be specified per solvent: the charge asymmetry  $p_{\text{cav}}$ , the electrostatic radius  $\eta$ , and the effective dispersion coefficient  $\sqrt{C_{\text{eff}}}$ .

The presence of ionic screening,  $k \neq 0$ , eliminates the indeterminacy of  $\phi(\mathbf{r})$  by an additive constant, establishing an absolute reference. It can be proven that the electrostatic potential decays to zero exponentially within the fluid far from the electronic system, where  $\rho_{\text{el}} = 0$ , so the zero of  $\phi(\mathbf{r})$  is not arbitrary but corresponds to the energy of a solvated electron within the solvent. [37] The absolute reference of the electrostatic potential allows for an absolute reference for the eigenvalues of the Kohn-Sham electronic states. Likewise, this means that the chemical potential,  $\mu$ , fixed in calculations and used to determine electronic occupations, is also aligned with the same reference. Values can be placed on the same scale using the experimental value of the absolute position of the standard hydrogen electrode relative to the vacuum level, namely  $\mu_{\text{SHE}} = -4.44 \text{ eV}$ . In the case of CANDLE, a theoretical calibration performed by Sundararaman and colleagues [60] which involves contrasting theoretical and experimental values of zero-charge potentials for solvated metal surfaces gives a value of  $\mu_{\text{SHE}} = -4.66 \text{ eV}$ . By using this value, one can align eigenvalues and chemical potentials, obtained using CANDLE as the model solvent, with respect to the standard hydrogen electrode potential.

## Quantum capacitance and softness of N-doped graphene within GCDFT

In recent years graphene has been found to be a very promising capacitor due to its properties such as high surface area, high electrical conductivity, low resistance, high mechanical strength, and chemical stability. Despite the efforts of researchers to develop theoretical models to understand the capacitance properties of

graphene, the fundamental factors governing its increased reactivity and the impacts of nonmetallic heteroatom doping remain uncertain. The absence of a thorough theoretical framework that comprises an electrified interface, a solvent under electric field influence, charge transfer mechanisms, adsorption phenomena among others is a significant factor. In terms of the application of functionalized graphene in electrochemical capacitors, one of the most important properties is the capacitance of the material. The total capacitance of a solid-liquid interface depends on the intrinsic capacitance of the solid surface and on what is identified as the double layer capacitance of the liquid in the vicinity of the surface. For the case of graphene-electrolyte interface, the dominant quantity is the intrinsic capacitance identified with the quantum capacitance, ( $C_{DOS}$ ), a concept introduced by Luryi[61] which characterizes the conduction band's mobility in response to an applied potential, hence the capacitance was a feature of electronic devices, later becoming a relevant factor for elucidating the fundamental chemistry aspects of electrode-electrolyte capacitors at their interface. Hwang and colleagues introduced an approach to calculate the total capacitance ( $C_T$ ) by separately analyzing quantum capacitance and electric double layer capacitance ( $C_{DL}$ ) on single-layer graphene.[62] Subsequently, Zhan and Jiang[63] studied the electronic structure of solvated few-layer graphene electrodes using JDFT within the grand canonical Kohn-Sham (GCKS) formalism. In that work they proposed a model of series capacitors and stated that employing the JDFT method would enable the separation and quantification of the dielectric contribution through a self-consistent electronic structure calculation for an electrode in contact with an implicit electrolyte. According to the Gouy-Chapman-Stern model,[64] the capacitance of the electrolyte component of a solid-electrolyte interface can be divided into the Helmholtz ( $C_H$ ) layer and the diffuse ( $C_{Df}$ ) layer contributions (See Fig. 4). To simplify matters, the combined Helmholtz and diffuse capacitances are often referred to as the electrolyte or double layer ( $1/C_{DL} \equiv 1/C_H + 1/C_{Df}$ ) capacitance. The Gouy-Chapman-Stern model provides an approximation for the  $C_{DL}$  term[64] and Monte Carlo simulations or classical molecular dynamics can yield a more comprehensive understanding of this contribution. [62,65,66] On the other hand, the contributions to total capacitance coming from the electrode can be divided into quantum capacitance, also known as DOS capacitance  $C_{DOS}$  and the dielectric capacitance  $C_{diel}$ . Thus, the total capacitance of a series capacitor model can be defined as

$$\frac{1}{C_T} = \underbrace{\frac{1}{C_{DL}}}_{\text{electrolyte}} + \underbrace{\frac{1}{C_{DOS}} + \frac{1}{C_{diel}}}_{\text{electrode}} \quad (27)$$

The quantum capacitance is conventionally derived from the rigid-band (RB) approximation:

$$C_{DOS}^{RB}(\Delta E_f) \approx \frac{e^2}{4k_B T} \int_{-\infty}^{\infty} g(E) \cosh^{-2} \left( \frac{E - (E_f^0 + \Delta E_f)}{2k_B T} \right) dE \quad (28)$$

where  $g(E)$  and  $E_f^0$  are the density of states and the Fermi level of the neutral electrode, respectively.  $\Delta E_f$  is the shift in the Fermi level of the charged electrode resulting from the variation of the total change in the electrochemical potential of the electrons. Through Zhan and Jiang's procedure,  $C_{DOS}$  is obtained from GCKS calculations, where the number of electrons is an average,  $\langle N \rangle$ , and the natural variables are the chemical potential of the electron reservoir,  $\mu$ , the external potential,  $V(\mathbf{r})$ , and the temperature. In this protocol, a change in the chemical potential of the electrons,  $\mu$ , can be separated in three contributions: 1) a shift in the Fermi level,  $\Delta E_f$ ; 2) a change in the electrostatic potential across the double layer,  $\Delta\Phi_{DL}$ , which is induced by the charging process of the electrode surface; 3) and the change in the chemical potential resulting from the penetration of the electric field into the semiconductor or non-conductor surface (the screening of metallic surfaces avoid this effect),  $\Delta\Phi_{diel}$ . Consequently, the change in the chemical potential can be written as:

$$\Delta\mu = \Delta E_f + \Delta\Phi_{DL} + \Delta\Phi_{diel} \quad (29)$$

It is important to notice that in series capacitors a change in the charge is replicated in each capacitor, therefore, the inverse of total capacitance can be split in contributions coming from each part of the total change in  $\mu$ . In Zhan and Jiang's model,[63]  $\Delta E_f$  corresponds to  $\frac{1}{C_{DOS}}$  and the dielectric and double layer terms are contained in a nonquantum term,  $\Delta\Phi_{NQ} = \Delta\Phi_{DL} + \Delta\Phi_{diel}$ . As a result, their model contains two terms,

$$\frac{1}{C_T} = \frac{1}{C_{DOS}} + \frac{1}{C_{NQ}} \quad (30)$$

that can be evaluated from a GCKS calculation of the solid-liquid interface using JDFT formalism.

The relation of the inverse of capacitance with a DFT response quantity, chemical hardness, was pointed out as earlier as 1988 by Perdew[67]; and this idea was further developed by others. [68,69] In addition, in 1985 Yang and Parr, using the GCDFT formalism, introduced a relation between changes in electron density relative to the chemical potential and the density of states (DOS) in metals with a response function called chemical softness.[40] Later on, Cohen et al. [70-73] have enhanced this association between local softness and local density of states, proposing an extension of this concept to semiconductor systems. As global and local quantities, softness and hardness are inverse at zero temperature[28] and have been widely used as reactivity parameters.[26] Moreover, a relationship between local softness and measurable quantities has been emphasized; on the one hand, a connection with scanning tunneling microscopy (STM) images was established which widened the applicability of atomic resolution STM images in studying surface reactivity; [74] on the other hand, more recently, Szareck[75] pointed out that global chemical softness is directly proportional and approximate to the total capacitance,

$$S \cong \frac{C_T}{e^2} \quad (31)$$

Since the total capacitance is the derivative of the electrode charge,  $e(\langle N \rangle - \langle N \rangle_0)$  with respect to chemical potential, it can be converted into a derivative with respect to the applied potential, U, through the expression  $\mu = \mu_0 - eU$ :

$$C_T = e^2 \frac{\partial(\langle N \rangle - \langle N \rangle_0)}{\partial \mu} \quad (32)$$

The rationale for this transformation is that the applied potential fixes the chemical potential of the electrons indicating that the electrode used to fix the potential acts as the electrons bath at a certain imposed chemical potential. Ochoa-Calle and colleagues[76] made a linkage between both methods to obtain quantum capacitance and softness using JDFT and CANDLE as implicit solvation model, to capture the charging process of the electrode by computing the curve  $\langle N \rangle$  vs  $\mu$ . They explored the relationship between capacitance and softness for pristine and N-substituted graphene structures (see Fig. 5) and defined a local total capacitance, alternative to the one proposed by Szareck,[75]

$$c_T(\mathbf{r}) \equiv e^2 S(\mathbf{r}) \quad (33)$$

They obtained that the rigid band approximation tends to overestimate quantum capacitance, especially in the pyridinic system, thereby reducing its impact on the total capacitance. With the model of series capacitors, they analyzed individually the  $\frac{1}{C_{DOS}}$  and  $\frac{1}{C_{NQ}}$  terms for the three systems, finding that for graphene, both of these terms are different in all of the studied applied potentials; for the positively charged N-doped systems, the nonquantum shift is analogous to the displacement of the Fermi level, whereas for the negatively charged pyridinic system the most important contribution is the nonquantum shift.

They compared the total capacitance of the three systems studied in their work (see Fig. 6), where they obtain that the pyridinic system has the greatest  $C_T$ , establishing the relative order as pyridinic bond type > graphitic bond type > graphene bond type. The curves depicted in Fig. 6, through Eq. 31 can also be understood as the global softness of the electrode-electrolyte system as a function of  $\mu$ . The N-doped systems have their local maxima in the potential region where they are prone to donate electrons. Additionally, Eq. 33 introduces the opportunity to establish local contributions to the  $C_T$ . For instance, they show that for the applied potential where there is the maximum peak of capacitance in the pyridinic system, the entire surface gives rise to the electron donation, whereas the heteroatoms are the only ones that contribute at the applied potential window where the system accepts electrons. It is important to notice, that the definition of global and local softnesses imply to take the derivatives at constant external potential, namely constant geometry. In contrast the derivative that defines capacitance, Eq. 32, is not taken with this restriction; this is the reason so that Eq. 31 is only an approximation. One of the advantages of the series capacitor model is that one can distinguish the quantum from the non-quantum contributions and to quantify their relative values. This possibility is useful to understand the performance of different materials in contact with the same solvent model.

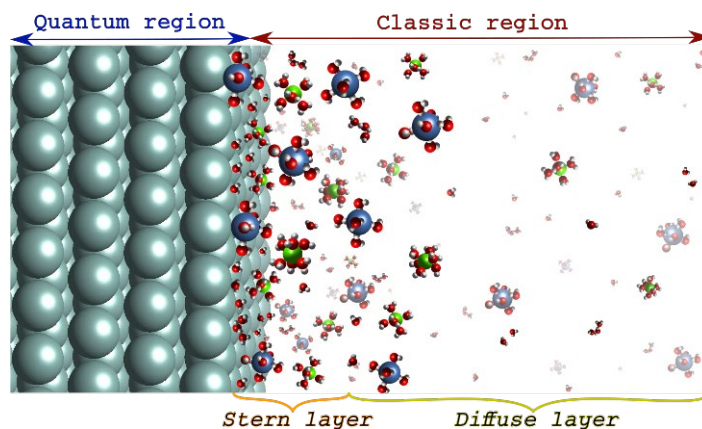


**Fig. 4.** Schematic representation of an electric double layer with green and blue spheres indicating solvated cation and anion, respectively.

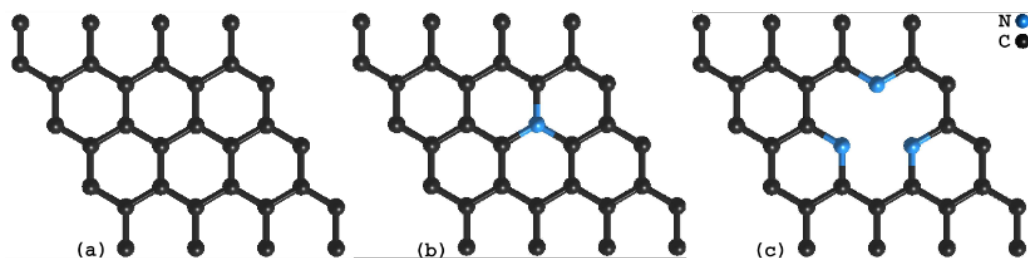


**Fig. 5.** N-doped structures with 0 %, 3.1 % and 9.7 % relative concentrations for (a) graphene, (b) graphitic bond type and (c) pyridinic bond type, respectively.

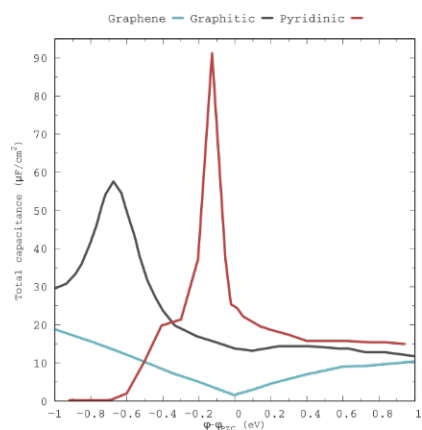


**Fig. 6.** Total capacitance of the three different N-doped models as a function of the applied chemical potential,  $\phi$ , referred to the chemical potential of zero charge,  $\phi_{PZC}$ . Pristine graphene is also included as a point of reference.

## Electronic structure and redox properties of metallic oxides as a function of the chemical potential

The advanced electrochemical oxidation processes (EAOPs)[77] are based on the generation of hydroxyl radicals, which exhibit high oxidative power and are capable of completely oxidizing organic contaminants to carbon dioxide and water. It is convenient because it operates close to standard ambient temperature and pressure, making it efficient for wastewater treatment. Boron-doped diamond (BDD) electrodes have proven effective in electrocombustion of organic compounds, achieving complete oxidation to  $\text{CO}_2$ . However, its use is hindered by high costs. Metal oxides have emerged as viable alternatives for this purpose. Understanding the interaction between metal oxides and water is an ongoing research endeavor, driven not only by the practical applications where these interactions are important but also by the theoretical and experimental challenges associated with their accurate characterization.

EAOP mechanism proposed by Comninellis[78] in acidic medium has as its first step the oxidation of water to form adsorbed hydroxyl radicals on the surface, according to the half reaction:



where M denotes the metallic site on the anode surface. The theoretical study of Comninellis mechanism initiated at UAMI group focused on determining surface reactions including the adsorption energies but using surface models in which the solvent was only marginally treated. [79,80] Recently, Islas-Vargas and colleagues[81] employed JDFT to study the first step of the mechanism (Eq. 34) on three metallic oxide surfaces,  $\text{PbO}_2$ ,  $\text{SnO}_2$  and  $\text{IrO}_2$ . These materials possess a common rutile-type structure and exhibit the most stable crystal face, the (110), which exhibits alternating rows of the unsaturated metal atom and bridging oxygen atoms (see Fig. 7). They carried out geometry optimizations using CANDLE as implicit solvation model, then they placed two explicit water molecules in the model slab to consider the hydrogen bonds established at the maximum coverage limit. In all three cases, the water molecules dissociated into OH on top of the metallic site and H bound to the bridging oxygen atom of the surface plane (see Fig. 8), as found in other works.[82]

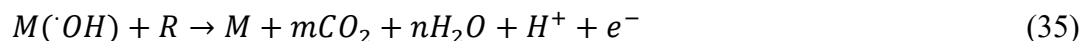
These three surfaces have diverse electronic behaviors. The density of states (DOS) of the slab models provides valuable understanding of the electronic properties of these metal oxides with two explicit water molecules. Specifically, it reveals that  $\text{PbO}_2$  exhibits a metallic behavior but with a limited number of electronic states around its Fermi level ( $E_f$ ), as shown in Fig. 9(a).  $\text{SnO}_2$  behaves as a semiconductor, with its potential of zero charge  $\mu_{zc}$  positioned in the midpoint of an approximated 1.22 eV bandgap, as seen in Fig. 9(b). In contrast to  $\text{PbO}_2$ ,  $\text{IrO}_2$  is a metallic system with a high density of states around the  $E_f$ , as depicted in Fig. 9(c).

At fixed geometry, Islas-Vargas et al. performed single point calculations employing GCDFT, fixing  $\mu$  around the  $\mu_{zc}$  of each slab model. They evaluated the difference between the average number of electrons and the number of electrons of the neutral system ( $\langle N \rangle - N_0$ ) as a function of the applied  $\mu$  (Fig. 10(a)) and the change of  $\langle N \rangle$  with respect to the applied chemical potential which represents the global softness (S) of the system (Fig. 10(b)) (see Eq. 4)

All chemical potentials are expressed as relative values, denoted as  $\mu - \mu_{SHE}$ , where  $\mu_{SHE}$  represents the energy value of the standard hydrogen electrode (SHE) relative to the vacuum level, which serves as the reference; in the case of CANDLE solvation model[60] the value was calibrated as -4.66 eV. Their results indicate that the two metallic systems present different responses before and after reaching their respective  $\mu_{zc}$ . When even a slight shift in  $\mu$  is applied, IrO<sub>2</sub> surface becomes more negatively or positively charged compared to PbO<sub>2</sub> which possesses a low density of states at  $E_f$ . Observing the global softness for these systems in Fig. 10(b), it suggests that the IrO<sub>2</sub> surface presents a pronounced response when the applied chemical potential lies in the direction of electron gain, whereas the PbO<sub>2</sub> surface presents equal propensity to either accept or donate electrons. In contrast, SnO<sub>2</sub> behaves as a semiconductor, lacking any change in the average number of electrons around its  $\mu_{zc}$  (see Fig. 10(a)), therefore presenting zero global softness until the applied  $\mu$  surpasses the bandgap.

Upon examining the alterations in the DOS at applied  $\mu$  (Fig. 11), two significant changes in the electronic structure of these materials become apparent: a shift of the entire DOS and its deformation. In the metallic systems, PbO<sub>2</sub> and IrO<sub>2</sub> (Fig. 11(a) and Fig. 11(c)), the shift in DOS is notably more pronounced compared to the system with a bandgap, SnO<sub>2</sub> (Fig. 11(b)), which exhibits a pronounced deformation rather than a substantial shift, once the  $\mu$  applied is outside the bandgap.

Islas-Vargas and colleagues[83] also investigated the chemical reactivity of these surfaces once an OH molecule was adsorbed, since these are the entities responsible for oxidizing organic molecules (R):[84]



They performed electronic structure calculations at fixed geometry using JDFT formalism and CANDLE as the implicit solvation model. Once optimized, they made single point calculations of the surfaces with an OH molecule at fixed  $\mu$ . The curve  $\langle N \rangle - N_0$  as a function of  $\mu$  referred to the  $\mu_{SHE}$  (Fig. 12(a)) indicates that these surfaces behave differently than those with two water molecules. In this case, all systems are metallic, and they exhibit a linear behavior in the potential region when  $\mu < \mu_{zc}$  and undergo a change in slope when  $\mu > \mu_{zc}$ . Both average number of electrons of the surfaces SnO<sub>2</sub> and PbO<sub>2</sub> with an OH molecule behave similarly in the applied potential window studied in their work. This can be explained by noting the similar characteristics of the electronic states associated with Sn and Pb, because they share common features as elements within the same group on the periodic table. Moreover, in accordance with a classification proposed by Cominellis,[78] PbO<sub>2</sub> and SnO<sub>2</sub> electrodes are categorized as “non active” materials, whereas IrO<sub>2</sub> is considered as an “active” material. This can be observed in the global softness that is illustrated in Fig. 12(b). All systems exhibit constant softness when  $\mu < \mu_{zc}$ , indicating a constant trend of electron loss in that potential region. The peaks of S for all three surfaces are in the electron-gaining zone when the applied  $\mu$  exceeds their respective  $\mu_{zc}$  values. The behavior of S for PbO<sub>2</sub> and SnO<sub>2</sub> surfaces display similar softness behaviors across the entire applied potential region, with peaks of similar values. In contrast, the IrO<sub>2</sub> surface exhibits a lower local peak magnitude, occurring at an applied chemical potential of more than 1 eV higher than the other two surfaces. These results are consistent with experimental observations. Therefore, the overpotential for the oxygen evolution reaction is -1.52 for IrO<sub>2</sub> and -1.90 eV for both SnO<sub>2</sub> and PbO<sub>2</sub> surfaces.[85] This implies that the “non active” surfaces exhibit a maximum S at more negative potentials compared to the “active” surfaces, similarly to their oxygen evolution overpotential, which is lower in eV.

To understand the regions involved in charge transfer during chemical potential changes they evaluated the local softness,  $S(\mathbf{r})$ .

They found that in the case of the “non active” materials when the applied  $\mu$  exceeds the  $\mu_{zc}$ , the local softness is predominantly located over the adsorbed OH molecule and the two oxygen atoms in the bridge position. As  $\mu$  rises, there is an increase in the average number of electrons leading to a greater negative charge on the surface and an increase in  $S(\mathbf{r})$ . However, even with the ongoing entry of electrons to the surface, the  $S(\mathbf{r})$  decreases indicating a loss in the ability to gain electrons on the OH molecule and on the O atoms in bridge

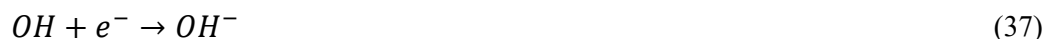
positions. Similarly, when  $\mu$  is greater than its  $\mu_{zc}$ , the local softness of the “active” material resides on the O atoms in bridge positions and on the O atom of the adsorbed OH. Nevertheless, with the increasing applied  $\mu$  the surface gains more electrons and the  $S(\mathbf{r})$  also increases until it reaches a certain value, at which it begins to decrease at a slower pace than the “non active” materials. The less pronounced decrease in local softness for the “active” material indicates that there are still available states on the surface O atoms as well as on the OH molecule to continue gaining electrons, in contrast to the “non active” surface.

**Absolute qualitative redox scale.** Theoretically, it is possible to split the total redox process and to study only one half-reaction:

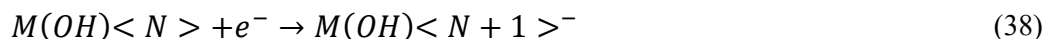


where  $m$  and  $\nu$  are integers with  $\nu > 0$ . Thus, in order to evaluate the oxidizing power of an electrode in relation to a particular electrochemical reaction, Islas-Vargas and colleagues[83] proposed a scale for the relative ordering of these surface materials. This scale can be employed as a tool to directly correlate with experimental measurements, expressed in Volts relative to the SHE, and to predict potential redox reactions. They took the works by Sprik et al.[1,2] who introduced a model for calculating reduction potentials in a grand canonical formulation where they only consider two states of the system of interest. By conducting molecular dynamics simulations, they take the average ground states while considering structural changes caused by thermal fluctuations. This methodology, termed *numerical titration*, involves iteratively adjusting  $\mu$  to determine its value at which the system exhibits half of its maximum fractional charge  $\mu_{1/2}$  from a sigma-shaped curve.

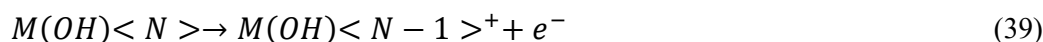
In the scheme proposed by Islas-Vargas et al.,[83] the equilibrium geometries of electronic systems in their respective ground states are employed. This enables calculations with fixed geometry while varying the chemical potential within the electrochemical window of experimental interest. They studied the reduction half-reaction of OH,



plotting the  $\langle N \rangle$  as a function of  $\mu$  and fitting this behavior to the function  $f(x) = (1 + e^{-a(x-b)})^{-1}$  as shown in Fig. 13. The calculated value of the reduction potential for OH/OH<sup>-</sup> is -1.42 eV, which deviates 480 meV from the experimental measure.[86] The deviation of theoretical values from the experimental ones is of the same order of magnitude as the one obtained by Sprik’s group. To test if the relative order of the redox potentials obtained with this approximation correlate with the experimental behavior, the group at UAMI used this approximation to determine the reduction potential  $\epsilon_{red}$  and the oxidation potential  $\epsilon_{ox}$  of surfaces with adsorbed OH, by considering the following half-reactions:



and



where  $M(OH)\langle N \rangle$ ,  $M(OH)\langle N + 1 \rangle^-$  and  $M(OH)\langle N - 1 \rangle^+$  are the states of the metallic oxide surface with an OH molecule with  $N$ ,  $N+1$  and  $N-1$  electrons, respectively. As in the OH/OH<sup>-</sup> case, they fitted the data of the  $\langle N \rangle - N_0 = f(\mu)$  curves (Fig. 12(a)). Additionally, they tried an alternative approach that involves determining the Helmholtz free energy at fixed values of electron number ( $N=N+1/2$  or  $N=N-1/2$ ). This approach entails obtaining the Helmholtz free energy at fractional electron numbers using the same Fermi-Dirac smearing function, rather than the grand potential. This procedure offers a more affordable alternative and enables the examination of a broader range of systems. The potentials derived through both methods are presented in Table 1; the qualitative trends of the data of the table are in agreement with the experimental results[87,88] a fact that supports the idea of using this qualitative scale to have a relative classification of the redox properties of solid-liquid interfaces.

**Table 1.** Oxidation potential ( $\epsilon_{ox}$ ) and reduction potential ( $\epsilon_{red}$ ) referred to the standard hydrogen electrode, in eV, for the  $MO_2(OH)$  (where  $M = Pb, Sn, Ir$ ) determined by two methods, I: interpolating the curves of  $\langle N \rangle - N_0 = f(\mu)$  in the -0.5 and 0.5 values and II: fixing  $N$  to be  $N+0.5$  or  $N-0.5$ , respectively.

	Method	$MO_2(OH)$		
		Pb	Sn	Ir
$\epsilon_{ox}$	I	-3.29	-3.37	-2.24
	II	-3.29	-3.37	-2.24
$\epsilon_{red}$	I	-2.37	-2.49	-0.49
	II	-2.39	-2.46	-0.92

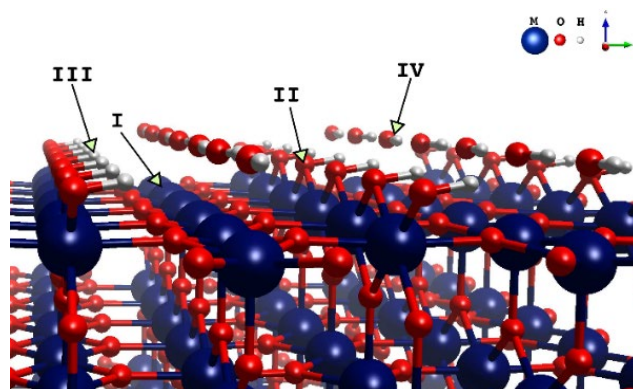


**Fig. 7.** Schematic representation of the (110)  $MO_2$  surface, where  $M = Pb, Sn,$  and  $Ir$ , with adsorbed dissociated water molecules. **I** unsaturated  $M$  atom where  $OH$  is adsorbed, **II** oxygen in bridge position, **III**  $H$  atom bound to the  $O$  atoms in bridge position and **IV** adsorbed  $OH$  molecule.

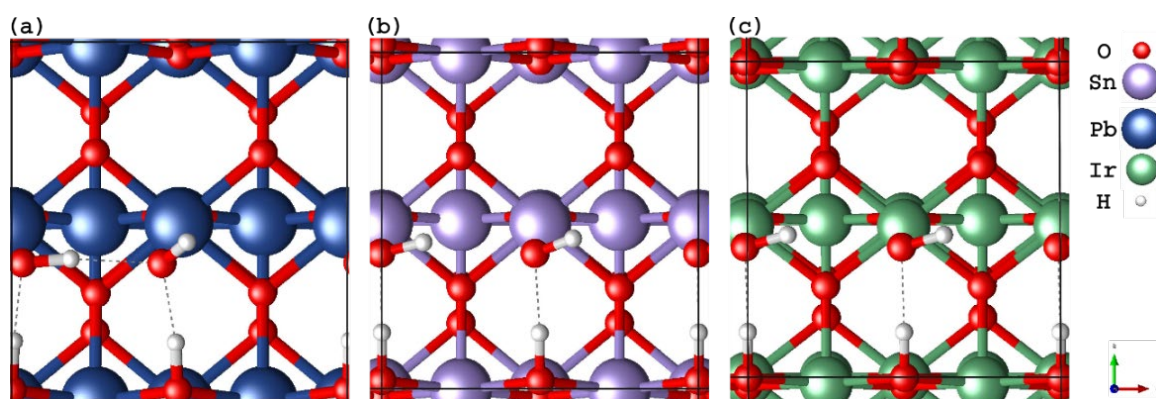


**Fig. 8.** Top view of the slab models with two explicit water molecules after geometry optimization with the CANDLE implicit solvation model and 1M of electrolyte, **(a)**  $PbO_2$ , **(b)**  $SnO_2$  and **(c)**  $IrO_2$ . Solid black lines delimit the unit cell.

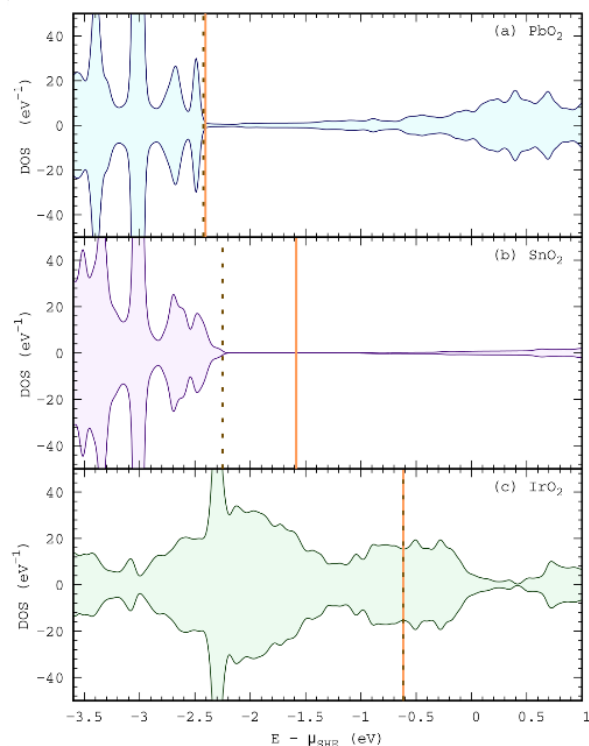


**Fig. 9.** Density of states per unit cell of the metal oxide surface models with two dissociated water molecules. The solid orange line and the dotted brown line represent the potential of zero charge ( $\mu_{zc}$ ) and the Fermi level ( $E_f$ ) of each slab, respectively.

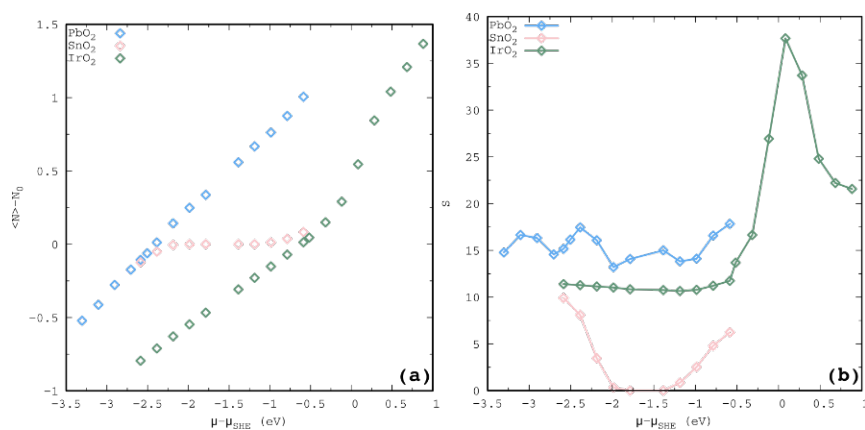


**Fig. 10.** (a) Average number of electrons difference,  $\langle N \rangle - N_0$ , at applied chemical potential in eV, where  $N_0$  is the number of electrons of the neutral system and (b) Softness in a.u. as a function of applied chemical potential, for the  $\text{MO}_2$  (with  $M = \text{Pb, Ir, and Sn}$ ) slab models with two explicit water molecules

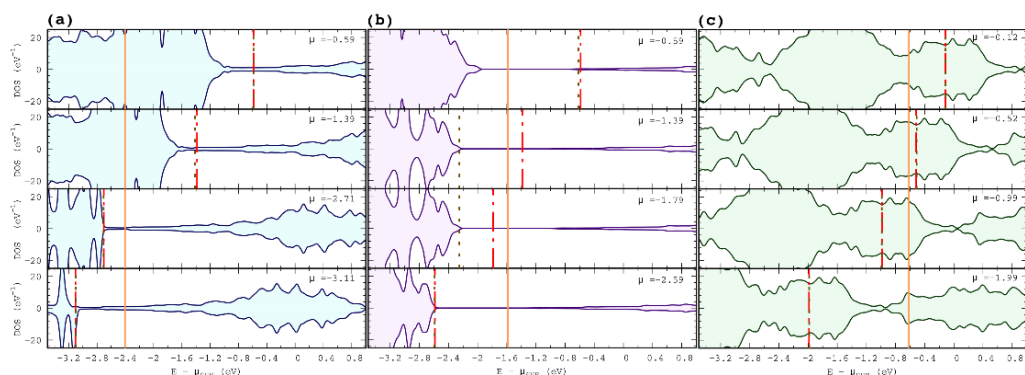


**Fig. 11.** Density of states per unit cell of the (a)  $\text{PbO}_2$ , (b)  $\text{SnO}_2$  and (c)  $\text{IrO}_2$  slab model with two explicit dissociated water molecules at applied chemical potential ( $\mu$ ) in eV. The orange solid line, dotted red line, and dotted brown line indicate  $\mu_{\text{ZC}}$ ,  $\mu$ , and the Fermi level, respectively.

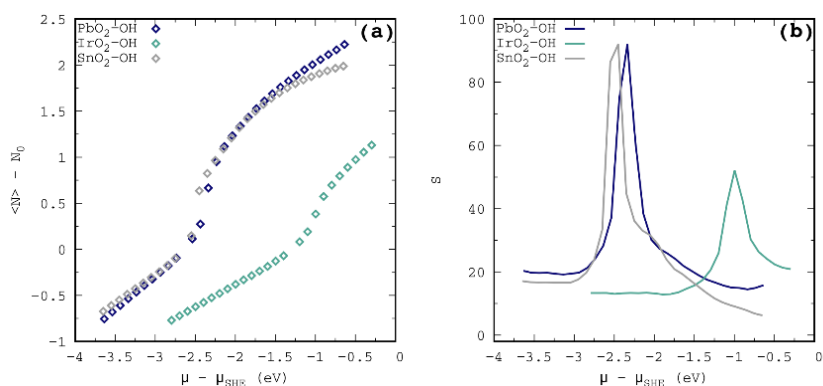


**Fig. 12.** (a) Average number of electrons difference,  $\langle N \rangle - N_0$ , at applied chemical potential in eV, where  $N_0$  is the number of electrons of the neutral system and (b) Softness in a.u. as a function of applied chemical potential, for the  $\text{MO}_2$  slab models with an OH molecule (with  $M = \text{Pb, Ir, and Sn}$ ).

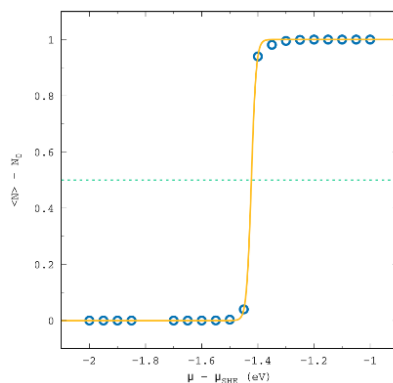


**Fig. 13.** Average number of electrons difference,  $\langle N \rangle - N_0$ , at applied chemical potential ( $\mu$ ), in eV, where  $N_0$  is the number of electrons of OH. Solid yellow line is the fitted function  $f(x) = (1 + e^{-a(x-b)})^{-1}$  with  $a = 118.529$  and  $b = -1.42318$ . Dotted green line indicates the gain of a half average electron.

## Conclusions

This review is focused on a significant area of research: the application of electronic structure calculations and reactivity concepts within DFT to analyze electrochemical processes. In particular, it was shown that the use of local softness as a probe to follow redox processes in cathode materials is an alternative to the standard use of projected density of states and simplifies the comparison of different materials without ambiguity. The development of quantum capacitance calculational procedures enhanced our understanding of electrode-electrolyte interfaces, particularly in materials like graphene; the connection between capacitance and softness opens the possibility of determining regional capacitances which facilitate the analysis of the impact of surface characteristics (functionalization, vacancies, etc.) to the global capacitance that is an experimentally measured quantity. Additionally, our research group, employing the grand canonical ensemble, has shed light on the surface properties of metallic oxides utilized in advanced electrochemical oxidation processes and their relative chemical reactivity order. This provides insights into possible redox reactions with organic compounds, which could facilitate the modification of these materials for wastewater treatment. Even though the Grand Canonical Finite Temperature Density Functional Theory is an exact theory, the following information must be considered. Similar to DFT, to obtain the Grand Potential in Eq. 2, the Kohn-Sham-Mermin formalism can be used to describe a system of interacting particles by introducing a fictitious system of non-interacting particles. Until this point, using this approach we still can get an exact solution for the Grand Potential, but in the way this theory is implemented in JDFTx these approximations are made: i) the entropic contribution to the Helmholtz energy is not exact because only the entropy of a system of non-interacting particles is included, the importance of this contribution and how it can be obtained is a current research topic [89-92]; ii) the exchange correlation functionals used are not exact, so the obtained results depend on the quality of the approximation and, also related to the unknown entropic contribution, the so called ground state approximation is used, i.e. the exchange-correlation free energy, that depends on the temperature, is approximated by its ground-state value[91]; iii) the solvation model used in JDFT[93]. Considering these issues in our works, we are aware of the limitations of PBE functional for describing the studied systems, that is why we usually prefer to analyze trends and not specific values. Analyzing the effect of a particular density functional approximation (DFA) is not straight forward in this formalism because the solvent model might need to be recalibrated for that DFA using experimental values. In summary, there is room for improvement on each one of the mentioned problems and this only reflects the great complexity involved in the study of electrochemical interfaces. Overall, the integration of theoretical approaches with solvent models and applied chemical potential continues to advance our comprehension of electrochemical processes and their correlation with experimental data, laying the groundwork for the design of more efficient electrode materials and the development of improved energy storage technologies.

## Acknowledgements

We want to thank CONAHCYT for financial support through projects CF-2023-G-1266 and FORDECYT PRONACES 1561802.

## References

1. Tavernelli, I.; Vuilleumier, R.; Sprik, M. *Phys. Rev. Lett.* **2002**, *88*, 213002. DOI: <https://doi.org/10.1103/PhysRevLett.88.213002>.
2. Tateyama, Y.; Blumberger, J.; Sprik, M.; Tavernelli, I. *J. Chem. Phys.* **2005**, *122*, 234505. DOI: <https://doi.org/10.1063/1.1938192>.
3. Sundararaman, R.; Vigil-Fowler, D.; Schwarz, K. *Chem. Rev.* **2022**, *122*, 10651-10674. DOI: <https://doi.org/10.1021/acs.chemrev.1c00800>.

4. Saubanière, M.; Yahia, M. B.; Lebègue, S.; Doublet, M. L. *Nature* **2014**, *5*, 5559. DOI: <https://doi.org/10.1038/ncomms6559>.
5. Neugebauer, H.; Bohle, F.; Bursch, M.; Hansen, A.; Grimme, S. *J. Phys. Chem. A* **2020**, *124*, 7166-7176. DOI: <https://doi.org/10.1021/acs.jpca.0c05052>.
6. Meng, Y. S.; Arroyo-de Dompablo, M. E. *Energ. Environ. Sci.* **2009**, *2*, 589-609. DOI: <https://doi.org/10.1039/b901825e>.
7. Li, M.; Yang, X.; Xue, Y. *Theor. Chem. Acc.* **2017**, *136*, 69. DOI: <https://doi.org/10.1007/s00214-017-2103-1>.
8. Jaque, P.; Marenich, A. V.; Cramer, C. J.; Truhlar, D. G. *J. Phys. Chem. C* **2007**, *111*, 5783-5799. DOI: <https://doi.org/10.1021/jp066765w>.
9. Fornari, R. P.; de Silva, P. *Molecules* **2021**, *26*, 3978. DOI: <https://doi.org/10.3390/molecules26133978>.
10. Fedorov, R.; Gryn'ova, G. *J. Chem. Theor. Comp.* **2023**, *19*, 4796-4814. DOI: <https://doi.org/10.1021/acs.jctc.3c00355>.
11. Cramer, C. J.; Truhlar, D. G. *Phys. Chem. Chem. Phys.* **2009**, *11*, 10757-10816. DOI: <https://doi.org/10.1039/b907148b>.
12. Bhattacharjee, S.; Isegawa, M.; Garcia-Ratés, M.; Neese, F.; Pantazis, D. A. *J. Chem. Theor. Comp.* **2022**, *18*, 1619-1632. DOI: <https://doi.org/10.1021/acs.jctc.1c01267>.
13. Arumugam, K.; Becker, U. *Minerals* **2014**, *4*, 345-387. DOI: <https://doi.org/10.3390/min4020345>.
14. Cheng, J.; Sulpizi, M.; Sprik, M. *J. Chem. Phys.* **2009**, *131*, 154504. DOI: <https://doi.org/10.1063/1.3250438>.
15. Blumberger, J.; Bernasconi, L.; Tavernelli, I.; Vuilleumier, R.; Sprik, M. *J. Am. Chem. Soc.* **2004**, *126*, 3928-3938. DOI: <https://doi.org/10.1021/ja0390754>.
16. Moens, J.; Jaque, P.; De Proft, F.; Geerlings, P. *J. Phys. Chem. A* **2008**, *112*, 6023-6031. DOI: <https://doi.org/10.1021/jp711652a>.
17. Moens, J.; Geerlings, P.; Roos, G. *Chemistry* **2007**, *13*, 8174-84. DOI: <https://doi.org/10.1002/chem.200601896>.
18. Miranda-Quintana, R. A.; Martínez Gonzalez, M.; Ayers, P. W. *Phys. Chem. Chem. Phys.* **2016**, *18*, 22235-22243. DOI: <https://doi.org/10.1039/c6cp03213c>.
19. Miranda, D. A.; Bueno, P. R. *Phys. Chem. Chem. Phys.* **2016**, *18*, 25984-25992. DOI: <https://doi.org/10.1039/c6cp01659f>.
20. Filhol, J. S.; Doublet, M. L. *J. Phys. Chem. C* **2014**, *118*, 19023-19031. DOI: <https://doi.org/10.1021/jp502296p>.
21. Feliciano, G. T.; Bueno, P. R. *J. Phys. Chem. C* **2020**, *124*, 14918-14927. DOI: <https://doi.org/10.1021/acs.jpcc.0c04598>.
22. Bueno, P. R.; Miranda, D. A. *Phys. Chem. Chem. Phys.* **2017**, *19*, 6184-6195. DOI: <https://doi.org/10.1039/c6cp02504h>.
23. Bueno, P. R.; Feliciano, G. T.; Davis, J. J. *Phys. Chem. Chem. Phys.* **2015**, *17*, 9375-9382. DOI: <https://doi.org/10.1039/c4cp06015f>.
24. Zheng, Y.; Jiao, Y.; Jaroniec, M.; Qiao, S. Z. *Angew. Chem. Int. Ed.* **2015**, *54*, 52-65. DOI: <https://doi.org/10.1002/anie.201407031>.
25. Parr, R. G.; Yang, W. *Density-Functional Theory of Atoms and Molecules*. New York: Oxford University Press, **1989**.
26. Geerlings, P.; De Proft, F.; Langenaeker, W. *Chem. Rev.* **2003**, *103*, 1793-1874. DOI: <https://doi.org/10.1021/cr990029p>.
27. Geerlings, P.; Chamorro, E.; Chattaraj, P. K.; De Proft, F.; Gázquez, J. L.; Liu, S.; Morell, C.; Toro-Labbé, A.; Vela, A.; Ayers, P. *Theor. Chem. Acc.* **2020**, *139*, 36. DOI: <https://doi.org/10.1007/s00214-020-2546-7>.
28. Gázquez, J. L.; Franco-Pérez, M.; Ayers, P. W.; Vela, A. *Int. J. Quantum Chem.* **2019**, *119*, e25797. DOI: <https://doi.org/https://doi.org/10.1002/qua.25797>.
29. Kohn, W.; Vashishta, P., in: *Theory of the Inhomogeneous Electron gas*, Lundqvist, S. and March, N. H. Eds., Plenum, New York, **1983**.

30. Mermin, N. D. *Phys. Rev.* **1965**, 137, A1441. DOI: <https://doi.org/10.1103/PhysRev.137.A1441>.
31. Sundararaman, R.; Schwarz, K. A.; Letchworth-Weaver, K.; Arias, T. A. *J. Chem. Phys.* **2015**, 142, 054102. DOI: <https://doi.org/10.1063/1.4906828>.
32. Sundararaman, R.; Letchworth-Weaver, K.; Schwarz, K. A. *J. Chem. Phys.* **2018**, 148, 144105. DOI: <https://doi.org/10.1063/1.5024219>.
33. Sundararaman, R.; Letchworth-Weaver, K.; Arias, T. A. *J. Chem. Phys.* **2014**, 140, 144504. DOI: <https://doi.org/10.1063/1.4870653>.
34. Sundararaman, R.; Arias, T. A. *Comput. Phys. Commun.* **2014**, 185, 818-825. DOI: <https://doi.org/10.1016/j.cpc.2013.11.013>.
35. Petrosyan, S. A.; Briere, J.-F.; Roundy, D.; Arias, T. A. *Phys. Rev. B.* **2007**, 75, 205105. DOI: <https://doi.org/10.1103/PhysRevB.75.205105>.
36. Mathew, K.; Sundararaman, R.; Letchworth-Weaver, K.; Arias, T. A.; Hennig, R. G. *J. Chem. Phys.* **2014**, 140, 084106. DOI: <https://doi.org/10.1063/1.4865107>.
37. Letchworth-Weaver, K.; Arias, T. A. *Phys. Rev. B.* **2012**, 86, 075140. DOI: <https://doi.org/10.1103/PhysRevB.86.075140>.
38. Gunceler, D.; Letchworth-Weaver, K.; Sundararaman, R.; Schwarz, K. A.; Arias, T. A. *Modell. Simul. Mater. Sci. Eng.* **2013**, 21, 074005. DOI: <https://doi.org/10.1088/0965-0393/21/7/074005>.
39. Franco-Pérez, M.; Gázquez, J. L.; Ayers, P. W.; Vela, A. *J. Chem. Phys.* **2015**, 143, 154103. DOI: <https://doi.org/10.1063/1.4932539>.
40. Yang, W.; Parr, R. G. *Proc. Natl. Acad. Sci. U.S.A.* **1985**, 82, 6723-6726. DOI: <https://doi.org/10.1073/pnas.82.20.6723>.
41. Vela, A.; Gázquez, J. L. *J. Am. Chem. Soc.* **1990**, 112, 1490-1492. DOI: <https://doi.org/10.1021/ja00160a029>.
42. Parr, R. G.; Yang, W. *J. Am. Chem. Soc.* **1984**, 106, 4049-4050. DOI: <https://doi.org/10.1021/ja00326a036>.
43. Goodenough, J. B. *Solid State Ionics.* **1994**, 69, 184-198. DOI: [https://doi.org/10.1016/0167-2738\(94\)90409-X](https://doi.org/10.1016/0167-2738(94)90409-X).
44. Armand, M. B., in: *Materials for Advanced Batteries*, Murphy, D. W., Broadhead, J., and Steele, B. C. H. Eds., Springer, **1980**, 145-161.
45. Kim, T.; Song, W.; Son, D.-Y.; Ono, L. K.; Qi, Y. *J. Mater. Chem. A.* **2019**, 7, 2942-2964. DOI: <https://doi.org/10.1039/C8TA10513H>.
46. Islas-Vargas, C.; Guevara-García, A.; Oliver-Tolentino, M.; Ramos-Sánchez, G.; González, I.; Galván, M. *J. Electrochem. Soc.* **2019**, 166, A5139. DOI: <https://doi.org/10.1149/2.0231903jes>.
47. Johannes, M.; Swider-Lyons, K.; Love, C. T. *Solid State Ionics.* **2016**, 286, 83-89. DOI: <https://doi.org/10.1016/j.ssi.2015.12.025>.
48. Johannes, M.; Hoang, K.; Allen, J.; Gaskell, K. *Phys. Rev. B.* **2012**, 85, 115106. DOI: <https://doi.org/10.1103/PhysRevB.85.115106>.
49. Perea-Ramírez, L. I.; Guevara-García, A.; Galván, M. *J. Mol. Model.* **2018**, 24, 227. DOI: <https://doi.org/10.1007/s00894-018-3754-0>.
50. Cohen, M. H.; Ganduglia-Pirovano, M. V.; Kudrnovský, J. *J. Chem. Phys.* **1994**, 101, 8988-8997. DOI: <https://doi.org/10.1063/1.468026>.
51. Hasan, M. H.; McCrum, I. T. *Curr. Opin. Electrochem.* **2022**, 33, 100937. DOI: <https://doi.org/10.1016/j.coelec.2022.100937>.
52. Zhang, Y.; Cummings, P. T. *ACS Appl. Mater. Interfaces.* **2019**, 11, 42680-42689. DOI: <https://doi.org/10.1021/acsami.9b09939>.
53. Sundararaman, R.; Goddard, W. A.; Arias, T. A. *J. Chem. Phys.* **2017**, 146, 114104. DOI: <https://doi.org/10.1063/1.4978411>.
54. Tomasi, J.; Mennucci, B.; Cammi, R. *Chem. Rev.* **2005**, 105, 2999-3094. DOI: <https://doi.org/10.1021/cr9904009>.

55. Klamt, A. *Wiley Interdiscip. Rev. Comput. Mol. Sci.* **2018**, *8*, e1338. DOI: <https://doi.org/10.1002/wcms.1338>.
56. Mennucci, B. *Wiley Interdiscip. Rev. Comput. Mol. Sci.* **2012**, *2*, 386-404. DOI: <https://doi.org/10.1002/wcms.1086>.
57. Cramer, C. J.; Truhlar, D. G. *Chem. Rev.* **1999**, *99*, 2161-2200. DOI: <https://doi.org/10.1021/cr960149m>.
58. Kohn, W.; Sham, L. J. *Phys. Rev.* **1965**, *140*, A1133. DOI: <https://doi.org/10.1103/PhysRev.140.A1133>.
59. Grimme, S. *J. Comput. Chem.* **2006**, *27*, 1787-1799. DOI: <https://doi.org/10.1002/jcc.20495>.
60. Sundararaman, R.; Goddard, W. A., 3rd. *J. Chem. Phys.* **2015**, *142*, 064107. DOI: <https://doi.org/10.1063/1.4907731>.
61. Luryi, S. *Appl. Phys. Lett.* **1988**, *52*, 501-503. DOI: <https://doi.org/10.1063/1.99649>.
62. Paek, E.; Pak, A. J.; Hwang, G. S. *J. Electrochem. Soc.* **2013**, *160*, A1. DOI: <https://doi.org/10.1149/2.019301jes>.
63. Zhan, C.; Jiang, D.-e. *J. Phys. Chem. Lett.* **2016**, *7*, 789-794. DOI: <https://doi.org/10.1021/acs.jpcclett.6b00047>.
64. Bard, A. J.; Faulkner, L. R. *Electrochemical Methods: Fundamentals and Applications*. Wiley, **2012**.
65. Bo, Z.; Li, C.; Yang, H.; Ostrikov, K.; Yan, J.; Cen, K. *Nano-Micro Lett.* **2018**, *10*, 33. DOI: <https://doi.org/10.1007/s40820-018-0188-2>.
66. Górnjak, R.; Lamperski, S. *J. Phys. Chem. C.* **2014**, *118*, 3156-3161. DOI: <https://doi.org/10.1021/jp411698w>.
67. Perdew, J. P. *Phys. Rev. B.* **1988**, *37*, 6175. DOI: <https://doi.org/10.1103/physrevb.37.6175>.
68. Sabin, J. R.; Trickey, S.; Apell, S. P.; Oddershede, J. *Int. J. Quantum Chem.* **2000**, *77*, 358-366. DOI: [https://doi.org/10.1002/\(SICI\)1097-461X\(2000\)77:1<358::AID-QUA35>3.0.CO;2-D](https://doi.org/10.1002/(SICI)1097-461X(2000)77:1<358::AID-QUA35>3.0.CO;2-D).
69. Iafrate, G.; Hess, K.; Krieger, J.; Macucci, M. *Phys. Rev. B.* **1995**, *52*, 10737. DOI: <https://doi.org/10.1103/physrevb.52.10737>.
70. Cohen, M. H.; Ganduglia-Pirovano, M. V.; Kudrnovský, J. *Phys. Rev. Lett.* **1994**, *72*, 3222-3225. DOI: <https://doi.org/10.1103/PhysRevLett.72.3222>.
71. Cohen, M.; Ganduglia-Pirovano, M.; Kudrnovský, J. *J. Chem. Phys.* **1994**, *101*, 8988-8997. DOI: <https://doi.org/10.1063/1.468026>.
72. Cohen, M. H.; Ganduglia-Pirovano, M. V.; Kudrnovský, J. *J. Chem. Phys.* **1995**, *103*, 3543-3551. DOI: <https://doi.org/10.1063/1.470238>.
73. Wilke, S.; Cohen, M. H.; Scheffler, M. *Phys. Rev. Lett.* **1996**, *77*, 1560-1563. DOI: <https://doi.org/10.1103/PhysRevLett.77.1560>.
74. Galvan, M.; Dal Pino Jr, A.; Wang, J.; Joannopoulos, J. D. *J. Phys. Chem.* **1993**, *97*, 783-785. DOI: <https://doi.org/10.1021/j100106a001>.
75. Szarek, P. *J. Phys. Chem. C.* **2016**, *120*, 17175-17183. DOI: <https://doi.org/10.1021/acs.jpcc.6b03752>.
76. Ochoa-Calle, A.; Guevara-García, A.; Vazquez-Arenas, J.; González, I.; Galván, M. *J. Phys. Chem. A.* **2020**, *124*, 573-581. DOI: <https://doi.org/10.1021/acs.jpca.9b10885>.
77. Pletcher, D., in: *Electrochemistry for the environment*, Comninellis, C. and Chen, G. Eds., Springer, **2010**.
78. Comninellis, C. *Electrochim. Acta.* **1994**, *39*, 1857-1862. DOI: [https://doi.org/10.1016/0013-4686\(94\)85175-1](https://doi.org/10.1016/0013-4686(94)85175-1).
79. Jaimes, R.; Vazquez-Arenas, J.; González, I.; Galván, M. *Electrochim. Acta.* **2017**, *229*, 345-351. DOI: <https://doi.org/10.1016/j.electacta.2017.01.120>.
80. Jaimes, R.; Vazquez-Arenas, J.; González, I.; Galván, M. *Surface Science.* **2016**, *653*, 27-33. DOI: <https://doi.org/10.1016/j.susc.2016.04.018>.
81. Islas-Vargas, C.; Guevara-García, A.; Galván, M. *J. Chem. Phys.* **2021**, *154*, 074704. DOI: <https://doi.org/10.1063/5.0035208>.
82. Ping, Y.; Sundararaman, R.; Goddard III, W. A. *Phys. Chem. Chem. Phys.* **2015**, *17*, 30499-30509. DOI: <https://doi.org/10.1039/c5cp05740j>.
83. Islas-Vargas, C.; Guevara-García, A.; Galván, M. *Theor. Chem. Acc.* **2024**, *143*, 34. DOI: <https://doi.org/10.1007/s00214-024-03103-2>.

84. Marselli, B.; Garcia-Gomez, J.; Michaud, P.-A.; Rodrigo, M. A.; Comminellis, C. *J. Electrochem. Soc.* **2003**, 150, D79. DOI: <https://doi.org/10.1149/1.1553790>.
85. Martinez-Huitle, C. A.; Ferro, S. *Chem. Soc. Rev.* **2006**, 35, 1324-1340. DOI: <https://doi.org/10.1039/b517632h>.
86. Koppenol, W.; Liebman, J. F. *J. Phys. Chem.* **1984**, 88, 99-101. DOI: <https://doi.org/10.1021/j150645a024>.
87. Berdinko, V.; Bazhin, N. *Russ. J. Phys. Chem.* **1970**, 44, 395.
88. Li, A.; Weng, J.; Yan, X.; Li, H.; Shi, H.; Wu, X. *J. Electroanal. Chem.* **2021**, 898, 115622. DOI: <https://doi.org/10.1016/j.jelechem.2021.115622>.
89. Smith, J. C.; Pribram-Jones, A.; Burke, K. *Phys. Rev. B.* **2016**, 93, 245131. DOI: <https://doi.org/10.1103/PhysRevB.93.245131>.
90. Harding, B. P.; Mauri, Z.; Xie, V. W.; Pribram-Jones, A. *J. Chem. Phys.* **2024**, 160, 154108. DOI: <https://doi.org/10.1063/5.0196650>.
91. Burke, K.; Smith, J. C.; Grabowski, P. E.; Pribram-Jones, A. *Phys. Rev. B.* **2016**, 93, 195132. DOI: <https://doi.org/10.1103/PhysRevB.93.195132>.
92. Kozłowski, J.; Perchak, D.; Burke, K. *arXiv preprint arXiv:2308.03319*. **2023**, DOI: <https://doi.org/10.48550/arXiv.2308.03319>.
93. Sundararaman, R.; Schwarz, K. *J. Chem. Phys.* **2017**, 146, 084111. DOI: <https://doi.org/10.1063/1.4976971>.